

PROBING THE SPINS OF SUPERMASSIVE BLACK HOLES WITH GRAVITATIONAL WAVES FROM SURROUNDING COMPACT BINARIES

BIN LIU^{1,2}, DONG LAI^{2,3}

¹ Niels Bohr International Academy, Niels Bohr Institute, Blegdamsvej 17, 2100 Copenhagen, Denmark

² Cornell Center for Astrophysics and Planetary Science, Department of Astronomy, Cornell University, Ithaca, NY 14853, USA

³ Tsung-Dao Lee Institute, Shanghai Jiao Tong University, Shanghai 200240, China

Draft version January 26, 2022

ABSTRACT

Merging compact black-hole (BH) binaries are likely to exist in the nuclear star clusters around supermassive BHs (SMBHs), such as Sgr A*. They may also form in the accretion disks of active galactic nuclei. Such compact binaries can emit gravitational waves (GWs) in the low-frequency band (0.001 – 1 Hz) that are detectable by several planned space-borne GW observatories. We show that the angular momentum vector of the compact binary (\mathbf{L}_{in}) may experience significant variation due to the frame-dragging effect associated with the spin of the SMBH. The dynamical behavior of \mathbf{L}_{in} can be understood analytically as a resonance phenomenon. We show that rate of change of \mathbf{L}_{in} encodes the information on the spin of the SMBH. Therefore detecting GWs from compact binaries around SMBHs, particularly the modulation of the waveform associated with the variation of \mathbf{L}_{in} , can provide a new probe on the spins of SMBHs.

Subject headings: binaries: general - black hole physics - gravitational waves - stars: black holes - stars: kinematics and dynamics

1. INTRODUCTION

The spins of the supermassive black holes (SMBHs) at the centers of galaxies are poorly constrained; this is the case even for Sgr A* in the Galactic Center (e.g., Ghez et al. 1998, 2008; Genzel et al. 2010). The spin vector of an accreting SMBH could in principle be constrained by modeling the accretion/radiation processes (e.g., Mościbrodzka et al. 2009; Broderick et al. 2011; Shcherbakov et al. 2012) and comparing with observations, such as those of Sgr A* and M87 from Event Horizon Telescope (e.g., Dexter et al. 2010; Broderick et al. 2016; Akiyama et al. 2019). The Galactic Center host a population of young massive stars (e.g., Genzel et al. 2000; Merritt 2013; Alexander 2017); it has been suggested that the relativistic frame dragging effect on their orbits could put constraints on the Sgr A*'s spin (e.g., Levin & Beloborodov 2003; Fragione & Loeb 2020).

Given the fact that the S-stars around Sgr A* are close to the SMBH ($\sim 0.01\text{pc}$, with the newly discovered S4714 orbit reaching a pericenter distance of 12.6AU; Gillessen et al. 2017; Abuter et al. 2019; Peißker et al. 2020), it is likely that binaries of compact objects could be present near SgrA* (e.g., Antonini & Perets 2012; Stephan et al. 2019). Similar compact binaries may also exist in nuclear star clusters around other SMBHs (e.g., O’Leary et al. 2009; Hopman 2009; Leigh et al. 2018) and/or form in disks of active galactic nuclei (e.g., McKernan et al. 2012; Bartos et al. 2017; Tagawa et al. 2020). These compact binaries may radiate gravitational waves (GWs) in the low-frequency band (0.001 – 1 Hz), which can be detectable by the planned/conceived space-borne GW observatories (e.g., Randall & Xianyu 2019b; Hoang et al.

2019; Deme et al. 2020), including LISA (e.g., Amaro-Seoane et al. 2017), TianQin (e.g., Luo et al. 2016), Taiji (e.g., Hu & Wu 2017), B-DECIGO (e.g., Nakamura et al. 2016), DeciHertz Observatories (e.g., Arca Sedda et al. 2019), and TianGO (e.g., Kuns et al. 2020). The orbital parameters for the barycenter motion of the compact binary around the SMBH can be extracted from the GW signal taking into account the phase change and Doppler shift (e.g., Inayoshi et al. 2017; Randall & Xianyu 2019a). A recent study (Yu & Chen 2021) has shown that the orientation change of orbital plane of the compact binary driven by the gravitational torque from the SMBH can be measurable for sources at distances less than 1 Gpc (depending on the assumed sensitivity of GW detectors). In this paper, we demonstrate that the spin of SMBH can significantly modify the orientation dynamics of the compact binary, even when the binary orbit remains circular (i.e., no Lidov-Kozai oscillations; see below). Therefore, in principle, detecting such compact binaries in GWs may provide a new probe to the spins of SMBHs, including that of SgrA*.

2. COMPACT BINARY NEAR A SPINNING SMBH

We consider a binary with masses m_1 , m_2 , semimajor axis a_{in} and eccentricity e_{in} , moving around a SMBH tertiary (m_3) on a wider orbit with a_{out} and e_{out} . The angular momenta of the inner and outer binaries are denoted by $\mathbf{L}_{\text{in}} \equiv L_{\text{in}} \hat{\mathbf{L}}_{\text{in}}$ and $\mathbf{L}_{\text{out}} \equiv L_{\text{out}} \hat{\mathbf{L}}_{\text{out}}$ (where $\hat{\mathbf{L}}_{\text{in}}$ and $\hat{\mathbf{L}}_{\text{out}}$ are unit vectors).

Gravitational perturbation from the SMBH make the inner binary precess, and may also induce Lidov-Kozai (LK) eccentricity oscillations if the mutual inclination

between $\hat{\mathbf{L}}_{\text{in}}$ and $\hat{\mathbf{L}}_{\text{out}}$ is sufficiently high. The relevant timescale is

$$t_{\text{LK}} = \frac{1}{\Omega_{\text{LK}}} = \frac{1}{n_{\text{in}}} \frac{m_{12}}{m_3} \left(\frac{a_{\text{out}} \sqrt{1 - e_{\text{out}}^2}}{a_{\text{in}}} \right)^3, \quad (1)$$

where $m_{12} \equiv m_1 + m_2$ and $n_{\text{in}} = (Gm_{12}/a_{\text{in}}^3)^{1/2}$ is the mean motion of the inner binary.

The first-order post-Newtonian (PN) theory introduces pericenter precession in both inner and outer binaries. In particular, the precession of the inner orbit competes with Ω_{LK} , and plays a crucial role in determining the maximum eccentricity e_{max} in LK oscillations (e.g., [Fabrycky & Tremaine 2007](#); [Liu et al. 2015](#)).

Since the tertiary mass m_3 is much larger than the masses of the inner binary, $m_3 \gg m_1, m_2$, several general relativity (GR) effects involving the SMBH can generate extra precessions on the binary orbits, and qualitatively change the dynamics (e.g., [Naoz et al. 2013](#); [Will 2014](#); [Liu et al. 2019](#); [Liu & Lai 2020](#)). In a systematic post-Newtonian framework of triple dynamics (e.g., [Will 2014](#); [Fang et al. 2019b](#); [Lim & Rodriguez 2020](#)), there are numerous terms. We summarize the most essential effects below (also the leading-order effects). The related equations are either from the classical work on binaries with spinning bodies (e.g., [Barker & O’Connell 1975](#)), or can be derived (or extended to include eccentricity) “by analogy”, i.e., by recognizing that the inner binary’s orbital angular momentum \mathbf{L}_{in} behaves like a “spin” ([Liu et al. 2019](#); [Liu & Lai 2020](#)). As we see below, the vector forms of the equations we use are much more transparent than the equations based on orbital elements (see [Will 2014](#); [Lim & Rodriguez 2020](#)), especially when dealing with misaligned \mathbf{L}_{in} , \mathbf{L}_{out} and \mathbf{S}_3 . Here, we consider the double-averaged (DA; averaging over both the inner and outer orbital periods) approximation, and present the secular equations of \mathbf{L}_{in} in vector forms. The coupled eccentricity equations for various GR effects are summarized in Appendix A.

(i) *Effect I: Precession of \mathbf{L}_{out} around \mathbf{S}_3 .* If the SMBH is rotating (with the spin angular momentum $\mathbf{S}_3 = \chi_3 Gm_3^2/c$, where $\chi_3 \leq 1$ is the Kerr parameter), \mathbf{L}_{out} experiences precession around \mathbf{S}_3 due to spin-orbit coupling if the two vectors are misaligned (1.5 PN effect) (e.g., [Barker & O’Connell 1975](#); [Fang & Huang 2019a](#))

$$\left. \frac{d\mathbf{L}_{\text{out}}}{dt} \right|_{\mathbf{L}_{\text{out}}\mathbf{S}_3} = \Omega_{\mathbf{L}_{\text{out}}\mathbf{S}_3} \hat{\mathbf{S}}_3 \times \mathbf{L}_{\text{out}}, \quad (2)$$

with

$$\Omega_{\mathbf{L}_{\text{out}}\mathbf{S}_3} = \frac{GS_3(4 + 3m_{12}/m_3)}{2c^2 a_{\text{out}}^3 (1 - e_{\text{out}}^2)^{3/2}}. \quad (3)$$

For the binary-SMBH system, \mathbf{S}_3 can be easily much larger than \mathbf{L}_{out} , and we can assume $\hat{\mathbf{S}}_3 = \text{constant}$.

(ii) *Effect II: Precession of \mathbf{L}_{in} around \mathbf{L}_{out} .* In addition to the Newtonian precession (driven by the tidal potential of m_3), \mathbf{L}_{in} experiences an additional de-Sitter like (geodesic) precession in the gravitational field of m_3 introduced by GR (1.5 PN effect), such that the net pre-

cession is governed by

$$\left. \frac{d\mathbf{L}_{\text{in}}}{dt} \right|_{\mathbf{L}_{\text{in}}\mathbf{L}_{\text{out}}} = \Omega_{\mathbf{L}_{\text{in}}\mathbf{L}_{\text{out}}} \hat{\mathbf{L}}_{\text{out}} \times \mathbf{L}_{\text{in}}, \quad (4)$$

with $\Omega_{\mathbf{L}_{\text{in}}\mathbf{L}_{\text{out}}} \equiv -\Omega_{\mathbf{L}_{\text{in}}\mathbf{L}_{\text{out}}}^{(\text{N})} (\hat{\mathbf{L}}_{\text{out}} \cdot \hat{\mathbf{L}}_{\text{in}}) + \Omega_{\mathbf{L}_{\text{in}}\mathbf{L}_{\text{out}}}^{(\text{GR})}$, and

$$\Omega_{\mathbf{L}_{\text{in}}\mathbf{L}_{\text{out}}}^{(\text{N})} = \frac{3}{4}\Omega_{\text{LK}}, \quad \Omega_{\mathbf{L}_{\text{in}}\mathbf{L}_{\text{out}}}^{(\text{GR})} = \frac{3}{2} \frac{G(m_3 + \mu_{\text{out}}/3)n_{\text{out}}}{c^2 a_{\text{out}} (1 - e_{\text{out}}^2)}, \quad (5)$$

where $n_{\text{out}} = (Gm_{\text{tot}}/a_{\text{out}}^3)^{1/2}$. Note that the Newtonian contribution to the precession rate neglects octuple and high-order terms; this is justified since dynamical stability of the triple requires $a_{\text{out}} \gg a_{\text{in}}$ when $m_3 \gg m_{12}$. For the GR part, high-order contributions to $\Omega_{\mathbf{L}_{\text{in}}\mathbf{L}_{\text{out}}}^{(\text{GR})}$ can be found in (e.g., [Will 2014](#); [Lim & Rodriguez 2020](#)).

(iii) *Effect III: Precession of \mathbf{L}_{in} around \mathbf{S}_3 .* Since the semimajor axis of the inner orbit (a_{in}) is much smaller than the outer orbit (a_{out}), the inner binary can be treated as a single body approximately. Thus, the angular momentum \mathbf{L}_{in} is coupled to the spin angular momentum \mathbf{S}_3 of m_3 , and experiences Lens-Thirring precession (2 PN effect).

$$\left. \frac{d\mathbf{L}_{\text{in}}}{dt} \right|_{\mathbf{L}_{\text{in}}\mathbf{S}_3} = \Omega_{\mathbf{L}_{\text{in}}\mathbf{S}_3} \hat{\mathbf{S}}_3 \times \mathbf{L}_{\text{in}} - 3\Omega_{\mathbf{L}_{\text{in}}\mathbf{S}_3} (\hat{\mathbf{L}}_{\text{out}} \cdot \hat{\mathbf{S}}_3) \hat{\mathbf{L}}_{\text{out}} \times \mathbf{L}_{\text{in}}, \quad (6)$$

where

$$\Omega_{\mathbf{L}_{\text{in}}\mathbf{S}_3} = \frac{GS_3}{2c^2 a_{\text{out}}^3 (1 - e_{\text{out}}^2)^{3/2}}. \quad (7)$$

Note that since the tertiary companion studied here is a SMBH, the binary embedded in the nuclear star cluster might also be influenced by the “environmental” effects, including binary evaporation (e.g., [Binney & Tremaine 1987](#)), resonant relaxation (e.g., [Hamers et al. 2018](#)), and non-spherical mass distribution (e.g., [Petrovich & Antonini 2017](#)). All these effects operate on timescales much longer than considered here and can be safely neglected.

3. ANALYTIC UNDERSTANDING OF \mathbf{L}_{in} EVOLUTION FOR CIRCULAR INNER BINARY

In [Liu et al. \(2019\)](#), we have examined how various GR effects modify the LK eccentricity evolution/growth of the inner binary and enhance the merger rate in the LIGO band. In [Liu & Lai \(2020\)](#), we have studied eccentricity growth due to apsidal precession resonance in nearly co-planar triple systems. Here, we focus on the dynamics of the inner binary far from merger, which radiates GW at low frequency band instead. Note that the evolution of \mathbf{L}_{in} is more sensitive to the SMBH spin than the orbital eccentricity. This is because the eccentricity excitation can be completely suppressed if the mutual inclination angle lies outside the LK window, or the binary is relatively far away from the SMBH.

To develop an analytic understanding of the dynamics of the binary-SMBH system, we first consider the case where the inner binary remains circular throughout the

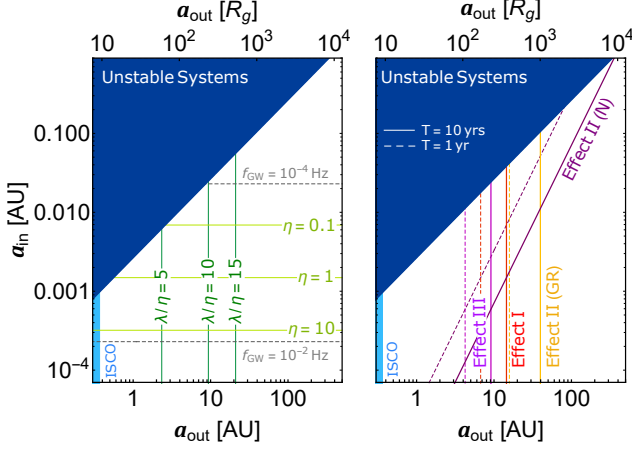


FIG. 1.— Parameter space in $a_{\text{in}} - a_{\text{out}}$ plane indicating the relative importance of various GR effects. The system parameters are $m_1 = 20M_\odot$, $m_2 = 10M_\odot$, $m_3 = 4 \times 10^6 M_\odot$, $e_{\text{in}} = 0$, $e_{\text{out}} = 0.5$ and $\chi_3 = 1$. The dark blue region corresponds to dynamically unstable triple systems (the instability limit according to Kiseleva et al. (1996)), and the light blue region indicates the innermost stable circular orbits (ISCO) for the outer binary, with $a_{\text{out}} \leq 9R_g = 9(Gm_3)/c^2$. In the left panel, the solid lines show different values of λ/η and η (evaluated using Eq. 11), and the dashed lines characterize the frequency of GWs emitted by the inner binary. In the right panel, the solid (dashed) lines are obtained by setting the relevant timescales (Eqs. 1, 3, 5 and 7) to 10 yrs (1 yr).

evolution. Since $\hat{\mathbf{L}}_{\text{out}}$ rotates around $\hat{\mathbf{S}}_3$ at a constant rate, $\Omega_{\text{L}_{\text{out}}\text{S}_3}$, it is useful to consider the evolution of $\hat{\mathbf{L}}_{\text{in}}$ in the frame corotating with $\hat{\mathbf{L}}_{\text{out}}$; Combining Eqs. (4), (2) and (6), we have

$$\left(\frac{d\hat{\mathbf{L}}_{\text{in}}}{dt}\right)_{\text{rot}} = \left\{ \left[\Omega_{\text{L}_{\text{in}}\text{L}_{\text{out}}} - 3\Omega_{\text{L}_{\text{in}}\text{S}_3} (\hat{\mathbf{L}}_{\text{out}} \cdot \hat{\mathbf{S}}_3) \right] \hat{\mathbf{L}}_{\text{out}} + \left(\Omega_{\text{L}_{\text{in}}\text{S}_3} - \Omega_{\text{L}_{\text{out}}\text{S}_3} \right) \hat{\mathbf{S}}_3 \right\} \times \hat{\mathbf{L}}_{\text{in}}. \quad (8)$$

The corresponding Hamiltonian is

$$\begin{aligned} \mathcal{H} = & -\frac{1}{2}\Omega_{\text{L}_{\text{in}}\text{L}_{\text{out}}}^{(\text{N})} (\hat{\mathbf{L}}_{\text{in}} \cdot \hat{\mathbf{L}}_{\text{out}})^2 + \Omega_{\text{L}_{\text{in}}\text{L}_{\text{out}}}^{(\text{GR})} (\hat{\mathbf{L}}_{\text{in}} \cdot \hat{\mathbf{L}}_{\text{out}}) \\ & + (\Omega_{\text{L}_{\text{in}}\text{S}_3} - \Omega_{\text{L}_{\text{out}}\text{S}_3}) (\hat{\mathbf{L}}_{\text{in}} \cdot \hat{\mathbf{S}}_3) \\ & - 3\Omega_{\text{L}_{\text{in}}\text{S}_3} (\hat{\mathbf{L}}_{\text{out}} \cdot \hat{\mathbf{S}}_3) (\hat{\mathbf{L}}_{\text{in}} \cdot \hat{\mathbf{L}}_{\text{out}}). \end{aligned} \quad (9)$$

We set up a coordinate system with $\hat{z} = \hat{\mathbf{L}}_{\text{out}}$, $\hat{y} \sin \alpha \equiv \hat{\mathbf{L}}_{\text{out}} \times \hat{\mathbf{S}}_3$, and let $\hat{\mathbf{L}}_{\text{in}} = \sin I (\cos \varphi \hat{x} + \sin \varphi \hat{y}) + \cos I \hat{z}$, where α is the angle between $\hat{\mathbf{L}}_{\text{out}}$ and $\hat{\mathbf{S}}_3$, and I is the angle between $\hat{\mathbf{L}}_{\text{in}}$ and $\hat{\mathbf{L}}_{\text{out}}$. The (dimensionless) Hamiltonian becomes

$$\begin{aligned} \bar{\mathcal{H}} = \frac{\mathcal{H}}{\Omega_{\text{L}_{\text{in}}\text{L}_{\text{out}}}^{(\text{N})}} = & -\frac{1}{2} \cos^2 I + \lambda \cos I \\ & -\frac{3}{4} \eta (2 \cos \alpha \cos I + \sin \alpha \sin I \cos \varphi), \end{aligned} \quad (10)$$

where we have introduced the dimensionless ratios

$$\lambda = \frac{\Omega_{\text{L}_{\text{in}}\text{L}_{\text{out}}}^{(\text{GR})}}{\Omega_{\text{L}_{\text{in}}\text{L}_{\text{out}}}^{(\text{N})}}, \quad \eta = \frac{\Omega_{\text{L}_{\text{out}}\text{S}_3}}{\Omega_{\text{L}_{\text{in}}\text{L}_{\text{out}}}^{(\text{N})}}, \quad (11)$$

and have used $\Omega_{\text{L}_{\text{in}}\text{S}_3}/\Omega_{\text{L}_{\text{out}}\text{S}_3} = (4 + 3m_{12}/m_3)^{-1} \simeq 1/4$. Note that $\cos I$ and φ are canonical variables.

Depending on the ratio of λ and η , we expect three possible $\hat{\mathbf{L}}_{\text{in}}$ behaviors¹: (i) For $|\lambda \pm 1| \gg \eta$ (“adiabatic”), $\hat{\mathbf{L}}_{\text{in}}$ closely follows $\hat{\mathbf{L}}_{\text{out}}$, maintaining an approximately constant I ; (ii) For $|\lambda \pm 1| \ll \eta$ (“nonadiabatic”), $\hat{\mathbf{L}}_{\text{in}}$ effectively precesses around $\hat{\mathbf{S}}_3$ with constant $\theta_{\text{L}_{\text{in}},\text{S}_3}$ (the angle between $\hat{\mathbf{L}}_{\text{in}}$ and $\hat{\mathbf{S}}_3$); (iii) When $|\lambda \pm 1| \sim \eta$ (“trans-adiabatic”), a resonance behavior of $\hat{\mathbf{L}}_{\text{in}}$ may occur, and large orbital inclination I can be generated.

Fig. 1 presents the parameter space indicating the relative importance of various GR effects for compact BH binaries (BHBs) around SgrA*. In the left panel, we see that for BHBs ($m_1 = 20M_\odot$ and $m_2 = 10M_\odot$) that radiate GWs in the low-frequency band ($10^{-4} - 10^{-2}\text{Hz}$), η ranges from 0.02 to 10. The “nonadiabatic” parameter regime ($\lambda \ll \eta$) is not allowed for the realistic systems because of the stability criterion and the effect of ISCO (Inner-most stable circular orbit). As a_{out} increases, λ/η increases and the dynamics of $\hat{\mathbf{L}}_{\text{in}}$ transitions from “trans-adiabatic” to “adiabatic”. Thus, resonance behavior of $\hat{\mathbf{L}}_{\text{in}}$ (i.e., $|\lambda \pm 1| \sim \eta$) can only occur when $\eta \lesssim 1$. In addition, to obtain variations of the orbit on relatively short timescales ($\lesssim 10\text{yrs}$; see the right panel of Fig. 1), the BHB cannot be too far away from the SMBH (i.e., $a_{\text{out}} \lesssim 50\text{AU}$).

Fig. 2 (panel A) illustrates how the GR effects induced by the spinning SMBH modify the evolution of $\hat{\mathbf{L}}_{\text{in}}$ of a BHB. We find that the orbital inclination I undergoes significant change due to the spin effects (Effects II-III; $\chi_3 = 1$), and the misalignment angles $\theta_{\text{L}_{x,y,z}}$ between $\hat{\mathbf{L}}_{\text{in}}$ and the fixed x, y, z axes exhibit dramatic oscillations. For reference, for a non-spinning SMBH, I stays constant and only regular oscillations of $\theta_{\text{L}_{x,y,z}}$ with small amplitude are produced.

Panel (C) of Fig. 2 shows the evolution of $\hat{\mathbf{L}}_{\text{in}}$ in the $(\varphi, \cos I)$ phase space. We see that the large variation of inclination is associated with the librating trajectory (i.e., resonance phenomenon), which is well described by the Hamiltonian (Eq. 10) with $\lambda = 0.74$ and $\eta = 0.057$.

As the BHB precesses, the GW waveform undergoes both amplitude and phase modulations, thereby allowing the measurement of the change in the orientation of $\hat{\mathbf{L}}_{\text{in}}$ (e.g., Yu & Chen 2021). Since $\theta_{\text{L}_{x,y,z}}$ evolves irregularly on the secular timescale that could be longer than the mission lifetime of future GW detectors (such as LISA), we recognize that the rate of change of $\hat{\mathbf{L}}_{\text{in}}$ (and of $\theta_{\text{L}_{x,y,z}}$) would be a useful observable indicator to track the evolution of the BHB. Fig. 3 shows the evolution of $d\theta_{\text{L}_{x,y,z}}/dt$ and $d\hat{\mathbf{L}}_{\text{in}}/dt$ for the example depicted in Fig. 2 (A). We see that the overall oscillations of $d\theta_{\text{L}_{x,y,z}}/dt$ and $d\hat{\mathbf{L}}_{\text{in}}/dt$ induced by the SMBH spin effects are more dramatic than the case without the spin effects, with $d\theta_{\text{L}_x}/dt$ and $d\hat{\mathbf{L}}_{\text{in}}/dt$ reaching an amplitude of $25^\circ/\text{yr}$ — Such a large and rapid change in $\hat{\mathbf{L}}_{\text{in}}$ leads

¹ Here we introduce λ and η to quantify the $\hat{\mathbf{L}}_{\text{in}}$ behavior and the resonance. Note that we have defined a similar factor γ in Liu et al. (2019), which involves the dependence on the inclination (I)

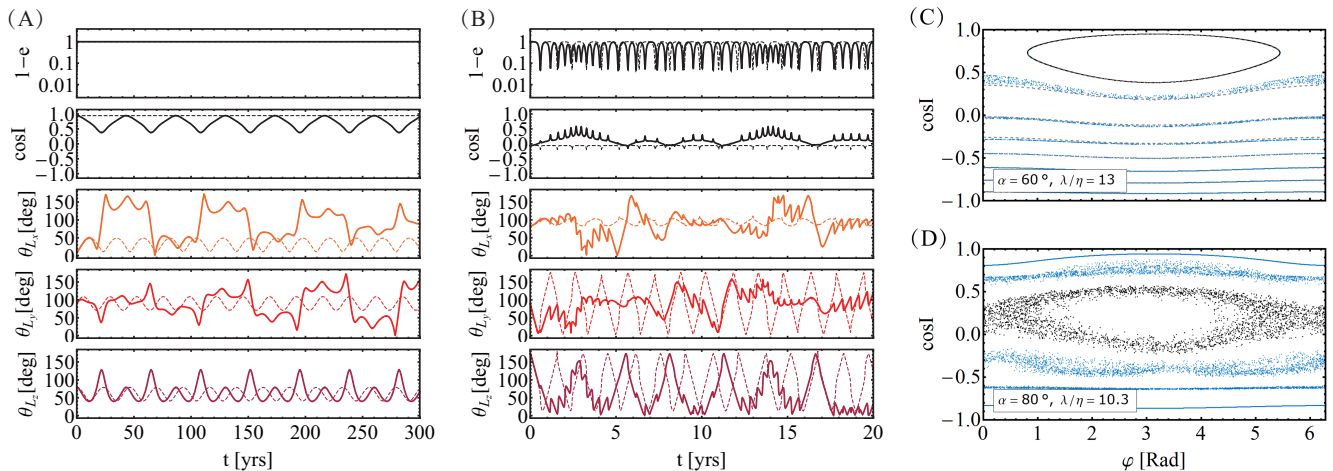


FIG. 2.— Sample eccentricity and angular momentum axis evolution of a BHB around a spinning SMBH tertiary. Panels (A) and (B) show the eccentricity, inclination (the angle between $\hat{\mathbf{L}}_{\text{in}}$ and $\hat{\mathbf{L}}_{\text{out}}$), and the misalignment angles between $\hat{\mathbf{L}}_{\text{in}}$ and the fixed x, y, z axes (where the z-axis is aligned with $\hat{\mathbf{S}}_3$ and the x-axis is in the initial $\hat{\mathbf{S}}_3 - \hat{\mathbf{L}}_{\text{out}}$ plane). The parameters are $m_1 = 20M_\odot$, $m_2 = 10M_\odot$, $a_{\text{in}} = 0.01\text{AU}$, $m_3 = 4 \times 10^6 M_\odot$, $e_{\text{in},0} = 0.001$, $e_{\text{out}} = 0.5$, $a_{\text{out}} = 15.8\text{AU}$, $I_0 = 19^\circ$, $\alpha = 60^\circ$ (panel A) and $a_{\text{out}} = 10\text{AU}$, $I_0 = 93.3^\circ$, $\alpha = 80^\circ$ (panel B). The solid/dashed trajectories represent the evolution with/without the effects included by the SMBH spin (Effects II-III). Panels (C) and (D) show the phase-space portraits obtained from the numerical integration (φ is the precessional phase of $\hat{\mathbf{L}}_{\text{in}}$ around $\hat{\mathbf{L}}_{\text{out}}$), where the black dots correspond to the examples in panels (A) and (B) and the blue dots are obtained for different values of initial inclinations (Panel (C): $I_0 = 79^\circ, 97^\circ, 109^\circ, 120^\circ, 131^\circ, 142^\circ, 156^\circ$; Panel (D): $I_0 = 20^\circ, 30^\circ, 102^\circ, 120^\circ, 150^\circ$). The dashed lines in panel (C) are contours of constant \mathcal{H} (Eq. 10) for a circular inner orbit (with $\lambda = 0.74$ and $\eta = 0.057$).

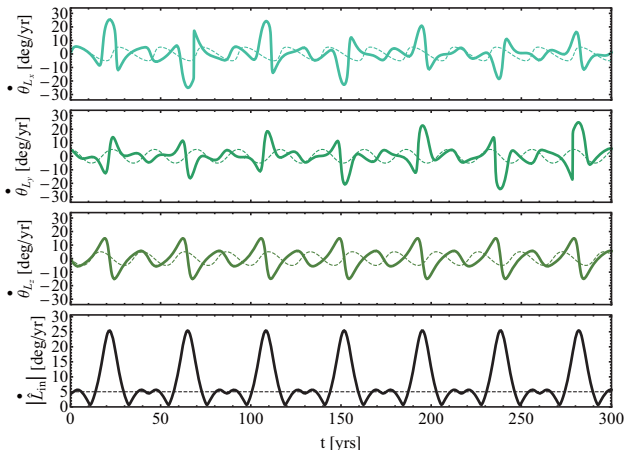


FIG. 3.— The rate of change of $\hat{\mathbf{L}}_{\text{in}}$ and the misalignment angles $\theta_{L_{x,y,z}}$ (the angle between $\hat{\mathbf{L}}_{\text{in}}$ and the fixed x, y, z axes) for the BHB evolution depicted in Fig. 2 (A). Here, the z-axis is along $\hat{\mathbf{S}}_3$, and the y-axis is along the initial $(\hat{\mathbf{S}}_3 \times \hat{\mathbf{L}}_{\text{out}})$ direction.

to significant amplitude modulation of the gravitational waveform, and should be easily detectable. In contrast, without the spin effects of the SMBH,

$$\left| \frac{d\hat{\mathbf{L}}_{\text{in}}}{dt} \right|_{\chi_3=0; e_{\text{in}}=0} = |\Omega_{L_{\text{in}}L_{\text{out}}}^{(\text{GR})} - \Omega_{L_{\text{in}}L_{\text{out}}}^{(\text{N})} \cos I_0| \sin I_0, \quad (12)$$

is a constant ($\simeq 5^\circ/\text{yr}$; see the bottom panel of Fig. 3).

4. GENERAL CASE

The BHB may experience eccentricity growth through LK oscillations when the inclination I is sufficiently large. The precession of $\hat{\mathbf{L}}_{\text{out}}$ around $\hat{\mathbf{S}}_3$ can increase the inclination window of eccentricity excitation (e.g., Liu et al.

2019). In this situation, the finite eccentricity of the inner binary increases the GW strain, which affects the overall signal-to-noise ratio and improves the detectability (e.g., Randall & Xianyu 2019b; Hoang et al. 2019; Deme et al. 2020).

The left panels of Fig. 4 show the maximum values of $d\theta_{L_{x,y,z}}/dt$, $|d\hat{\mathbf{L}}_{\text{in}}/dt|$ and the maximum eccentricity e_{max} as a function of the initial inclination I_0 for the same system parameters as in Fig. 2 (A). We see that in the absent of spin effects (purple dots), the maximum rates and eccentricity are uniquely determined by I_0 , and $|d\hat{\mathbf{L}}_{\text{in}}/dt|$ agrees with Eq. (12) for a wide range of I_0 even when the inner binary develops eccentricities (this arises because $|d\hat{\mathbf{L}}_{\text{in}}/dt|_{\text{max}}$ is achieved when $e_{\text{in}} \simeq 0$ during the LK cycles). However, with the inclusion of the SMBH spin effects (cyan dots), the eccentricity excitation window is widen (e.g., Liu et al. 2019), and there can be a finite spread of the maximum values of $|d\theta_{L_{x,y,z}}/dt|$ and $|d\hat{\mathbf{L}}_{\text{in}}/dt|$ for each I_0 . Note that for systems with $e_{\text{max}} \lesssim 0.6$, the dynamics of $\hat{\mathbf{L}}_{\text{in}}$ can still be described approximately in an analytical way, using the ‘‘circular’’ Hamiltonian (Eq. 10). This has been seen in Fig. 2 (C): the numerical trajectories (blue dots) are close to the analytical $\mathcal{H} = \text{constant}$ curves.

To explore the dependence of the direction of $\hat{\mathbf{S}}_3$ on the evolution of $\hat{\mathbf{L}}_{\text{in}}$, we consider a different α value ($= 85^\circ$), and the results are shown in the right panels of Fig. 4. Similar distributions are obtained, except that the e -excitation window is broader than the $\alpha = 60^\circ$ case shown in the left panel (see more details in the Supplemental Material).

The eccentricity excitation can be more significant if the BHB is closer to the SMBH. At the same time, the

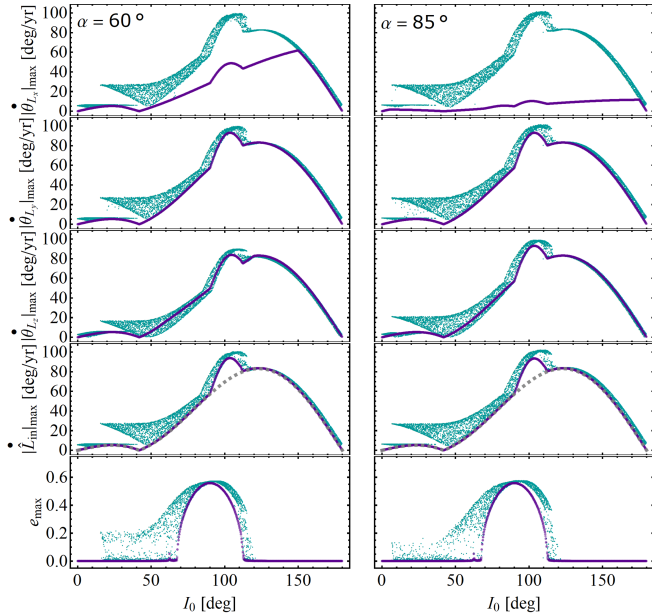


FIG. 4.— Maximum rates of change of $\theta_{Lx,y,z}$, $\hat{\mathbf{L}}_{\text{in}}$ and the maximum eccentricity of the inner BHB vs. the initial inclination I_0 for two different misalignment angle between $\hat{\mathbf{S}}_3$ and \mathbf{L}_{out} (α ; as labeled). The inner binary has $m_1 = 20M_\odot$, $m_2 = 10M_\odot$, $a_{\text{in}} = 0.01\text{AU}$, and the SMBH has $m_3 = 4 \times 10^6 M_\odot$, $e_{\text{out}} = 0.5$ and $a_{\text{out}} = 15.8\text{AU}$ (the initial eccentricity $e_{\text{in}} = 0.001$). Each I_0 is simulated ten times, with the initial orbital elements (the arguments of pericenters, the longitudes of the ascending nodes and the azimuthal phase angle of $\hat{\mathbf{S}}_3$) chosen randomly from 0 to 2π for each integration. We evolve the DA secular equations for the triple systems for 2000 yrs. The purple (cyan) dots are the results without (with) the SMBH spin effects. The dashed lines in the panels of $|\dot{\hat{\mathbf{L}}}_{\text{in}}|_{\text{max}}$ are from Eq. (12) assuming circular inner binary and non-spinning SMBH.

precession timescales become shorter and a wide range of variations of the BHB orbit can be potentially captured during the observational span of a few years. Panel (B) of Fig. 2 shows the example with $a_{\text{out}} = 10\text{AU}$. We see that because of the SMBH spin effects, the normal periodic oscillations in e and $\cos I$ transform into irregular oscillations. In this case, the “circular” Hamiltonian (Eq. 10) no longer applies. Instead, as indicated in panel (D) of Fig. 2, a large degree of scatter fills up the phase space, and the variation of $\hat{\mathbf{L}}_{\text{in}}$ becomes chaotic (see Appendix B).

5. SUMMARY AND DISCUSSION

We have studied the effects of the spin of SMBH (such as SgrA*) on the evolution of the orbital axis ($\hat{\mathbf{L}}_{\text{in}}$) of surrounding compact binaries. We find that for typical BHBs ($m_1 \sim 20M_\odot$ and $m_2 \sim 10M_\odot$) that are close to the SMBH ($a_{\text{out}} \lesssim 50\text{AU}$), $\hat{\mathbf{L}}_{\text{in}}$ may experience complex (and even resonant) evolution, leading to significant variation of $\hat{\mathbf{L}}_{\text{in}}$. For the BHBs that remain circular during the evolution, this variation of $\hat{\mathbf{L}}_{\text{in}}$ can be calculated analytically. We show that a spinning SMBH can greatly influence the variation of $\hat{\mathbf{L}}_{\text{in}}$ (even for the circular BHBs), increasing $|d\hat{\mathbf{L}}_{\text{in}}/dt|$ significantly compared to the case of a non-spinning SMBH. The maximum $|d\hat{\mathbf{L}}_{\text{in}}/dt|$ can

reach many tens of degrees per year for BHBs emitting GWs in the low-frequency band ($10^{-3} - 10^{-1}\text{Hz}$). Such rapid variation of $\hat{\mathbf{L}}_{\text{in}}$ therefore provides a probe on the mass and spin of the SMBH.

The SMBH spin can also affect other type of compact binaries, including neutron star binaries and white dwarf binaries. Although there is no direct observational evidence for their existence near SgrA*, massive stars with distances within $\sim 13\text{AU}$ from SgrA* are known (e.g., Gillessen et al. 2017; Abuter et al. 2019; Peißker et al. 2020), and it is plausible to expect stellar binaries their remnants to exist at such distances. In addition, various dynamical processes can lead to enhanced production of compact binaries around SMBHs, including gravitational bremsstrahlung (e.g., O’Leary et al. 2009), mass segregation (e.g., Antonini & Rasio 2016; Leigh et al. 2018; Fragione & Sari 2018; Sari & Fragione 2019; Arca Sedda et al. 2020), scatterings via eccentric disks (e.g., Generozov & Madigan 2020), and tidal/GW capture (e.g., Chen & Han 2020).

For the detectability in GWs, the types of compact binaries studied here are luminous low-frequency GW sources in the Galaxy (e.g., the signal-to-noise ratio $\gtrsim 37$ with LISA’s sensitivity; see also Appendixes C and D). Since the orbital period of the outer binary is much shorter than the duration of GW detection, the system parameters can be well constrained through Doppler phase shift (e.g., Inayoshi et al. 2017; Randall & Xi- anyu 2019a). Detecting the GW signal containing the signature of the frame-dragging effect is more challenging. A recent study (Yu & Chen 2021) (which neglects the frame-dragging effect) found that the regular precession of \mathbf{L}_{in} around \mathbf{L}_{out} due to Newtonian torques can be measurable if the precession period is less than the observation time. Similar detectability is expected to apply for the non-regular evolution of $\hat{\mathbf{L}}_{\text{in}}$ discussed in this paper. If the system happens to be observed during the time when $|d\hat{\mathbf{L}}_{\text{in}}/dt|$ is significantly enhanced, the effect would be more “visible”.

To conclude, our proof-of-concept calculations demonstrate that the SMBH spin can have large imprint on the BHB waveforms. A joint detection of multiple compact binary systems may be necessary to reduce the degeneracy of the GW signals on various parameters, and provide sufficient constraints on the SMBH spin. Future studies on detailed strategy to measure the SMBH spin using low-frequency GWs from compact binaries would be of great value.

6. ACKNOWLEDGMENTS

BL thank Johan Samsing and Daniel D’Orazio for useful discussion. DL has been supported in part by NSF grants AST-1715246 and AST-2107796. This project has received funding from the European Union’s Horizon 2020 research and innovation program under the Marie Skłodowska-Curie grant agreement No. 847523 ‘INTER-ACTIONS’.

REFERENCES

- Alexander, T. 2017, *ARA&A*, 55, 17
Amaro-Seoane, P., Audley, H., Babak, S., et al. 2017, arXiv e-prints, arXiv:1702.00786
Antonini, F. & Perets, H. B. 2012, *ApJ*, 757, 27
Antonini, F. & Rasio, F. A. 2016, *ApJ*, 831, 187
Arca Sedda, M., et al. 2019, arXiv e-prints, arXiv:1908.11375
Arca Sedda, M. 2020, *ApJ*, 891, 47
Barker, B. M., & O’Connell, R. F. 1975, *PhRvD*, 12, 329
Bartos, I., Kocsis, B., Haiman, Z., & Márka, S. 2017, *ApJ*, 835, 165
Binney, J., & Tremaine, S. 1987, *Galactic dynamics* (Princeton, NJ: Princeton Univ. Press)
Broderick A. E., Fish V. L., Doeleman S. S., & Loeb A. 2011, *ApJ*, 735, 110
Broderick, A. E., Fish, V. L., Johnson, M. D., et al. 2016, *ApJ*, 820, 137
Chen, X. & Han, W.-B. 2018, *Communications Physics*, 1, 53
Deme, B., Hoang, B.-M., Naoz, S., & Kocsis, B. 2020, *ApJ*, 901, 125
Dexter, J., Agol, E., Fragile, P. C., & McKinney, J. C. 2010, *ApJ*, 717, 1092
Event Horizon Telescope Collaboration, Akiyama, K., Alberdi, A., et al. 2019, *ApJL*, 875, L1
Fabrycky, D., & Tremaine, S. 2007, *ApJ*, 669, 1298
Fang, Y., & Huang, Q.-G. 2019a, *PhRvD*, 99, 103005
Fang, Y., Chen, X., & Huang, Q.-G. 2019b, *ApJ*, 887, 210
Fragione, G. & Sari, R. 2018, *ApJ*, 852, 51
Fragione, G. & Loeb A. 2020, *ApJ*, 901, L32
Generozov, A., & Madigan, A.-M. 2020, *ApJ*, 896, 137
Genzel R., Pichon C., Eckart A., Gerhard O.E., & Ott T., 2000, *MNRAS*, 317, 348
Genzel, R., Eisenhauer, F., & Gillessen, S. 2010, *Reviews of Modern Physics*, 82, 3121
Ghez, A. M., Klein, B. L., Morris, M., et al. 1998, *ApJ*, 509, 678
Ghez, A. M., Salim, S., Weinberg, N. N., et al. 2008, *ApJ*, 689, 1044
Gillessen, S., Plewa, P. M., Eisenhauer, F., et al. 2017, *ApJ*, 837, 30
Gravity Collaboration; Abuter, R., Amorim, A., Berger, J. P., et al. 2019, *A&A*, 625, L10
Hamers, A. S., Bar-Or, B., Petrovich, C., & Antonini, F. 2018, *ApJ*, 865, 2
Hoang, B.-M., Naoz, S., Kocsis, B., Farr, W. M., & McIver, J. 2019, *ApJL*, 875, L31
Hopman, C. 2009, *ApJ*, 700, 1933
Hu, W.-R., & Wu, Y.-L. 2017, *NAsRev*, 4, 685
Inayoshi, K., Tamanini, N., Caprini, C., & Haiman, Z. 2017, *PhRvD*, 96, 063014
Kiseleva, L. G., Aarseth, S. J., Eggleton, P. P., & de La Fuente Marcos, R. 1996, in *ASP Conf. Ser. 90, The Origins, Evolution, and Destinies of Binary Stars in Clusters*, ed. E. F. Milone & J.-C. Mermilliod (San Francisco, CA: ASP), 433
Kuns, K. A., Yu, H., Chen, Y., & Adhikari, R. X. 2020, *PhRvD*, 102, 043001
Leigh, N. W. C., Geller, A. M., McKernan, B., et al. 2018, *MNRAS*, 474, 5672
Levin, Y., & Beloborodov, A. M. 2003, *ApJL*, 590, L33
Lim, H., & Rodriguez, C. L. 2020, *PhRvD*, 102, 064033
Liu, B., Muñoz, D. J., & Lai, D. 2015, *MNRAS*, 447, 747
Liu, B., Lai, D., & Wang, Y.-H. 2019, *ApJL*, 883, L7
Liu, B., & Lai, D. 2020, *PhRvD*, 102, 023020
Luo, J., Chen, L.-S., Duan, H.-Z., et al. 2016, *Classical and Quantum Gravity*, 33, 035010
McKernan, B., Ford, K. E. S., Lyra, W., & Perets, H. B. 2012, *MNRAS*, 425, 460
Merritt, D. 2013, *Dynamics and Evolution of Galactic Nuclei*
Mościbrodzka, M., Gammie, C. F., Dolence, J. C., Shiokawa, H., & Leung, P. K. 2009, *ApJ*, 706, 497
Nakamura, T., et al. 2016, *PTEP*, 2016, 093E01
Naoz, S., Kocsis, B., Loeb, A., & Yunes, N. 2013, *ApJ*, 773, 187
O’Leary, R. M., Kocsis, B., & Loeb, A. 2009, *MNRAS*, 395, 2127
Peißker, F., Eckart, A., Zajaček, M., Ali, B., & Parsa, M. 2020, *ApJ*, 899, 50
Petrovich, C., & Antonini, F. 2017, *ApJ*, 846, 146
Randall, L., & Xianyu, Z.-Z. 2019a, *ApJ*, 878, 75
Randall, L., & Xianyu, Z.-Z. 2019b, arXiv e-prints, arXiv:1902.08604
Robson, T., Cornish, N. J., & Liu, C. 2019, *Classical and Quantum Gravity*, 36, 105011
Sari, R., & Fragione, G. 2019, *ApJ*, 885, 24
Shcherbakov, R. V., Penna, R. F., & McKinney, J. C. 2012, *ApJ*, 755, 133
Stephan, A. P., Naoz, S., Ghez, A. M., et al. 2019, *ApJ*, 878, 58
Tagawa, H., Haiman, Z., & Kocsis, B. 2020, *ApJ*, 898, 25
Will, C. M. 2014, *PhRvD*, 89, 044043
Yu, H., & Chen, Y. 2021, *PhRvL*, 126, 021101

APPENDIX

A: GR EFFECTS DUE TO ROTATING SMBH

We summarize the most essential GR effects for the BHB-SMBH triple system below. The related equations follow from the double-averaged (DA; averaging over both the inner and outer orbital periods) approximation.

(i) *Effect I: Precession of \mathbf{L}_{out} around \mathbf{S}_3 .* In the BHB-SMBH system, the angular momentum of the outer binary \mathbf{L}_{out} and the spin angular momentum \mathbf{S}_3 of m_3 precesses around each other due to spin-orbit coupling if the two vectors are misaligned (1.5 PN effect) (e.g., [Barker & O’Connell 1975](#); [Fang & Huang 2019a](#)):

$$\left. \frac{d\mathbf{L}_{\text{out}}}{dt} \right|_{\mathbf{L}_{\text{out}}\mathbf{S}_3} = \Omega_{\mathbf{L}_{\text{out}}\mathbf{S}_3} \hat{\mathbf{S}}_3 \times \mathbf{L}_{\text{out}}, \quad (\text{A1})$$

$$\left. \frac{d\mathbf{e}_{\text{out}}}{dt} \right|_{\mathbf{L}_{\text{out}}\mathbf{S}_3} = \Omega_{\mathbf{L}_{\text{out}}\mathbf{S}_3} \hat{\mathbf{S}}_3 \times \mathbf{e}_{\text{out}} - 3\Omega_{\mathbf{L}_{\text{out}}\mathbf{S}_3} (\hat{\mathbf{L}}_{\text{out}} \cdot \hat{\mathbf{S}}_3) \hat{\mathbf{L}}_{\text{out}} \times \mathbf{e}_{\text{out}}, \quad (\text{A2})$$

$$\left. \frac{d\hat{\mathbf{S}}_3}{dt} \right|_{\mathbf{S}_3\mathbf{L}_{\text{out}}} = \Omega_{\mathbf{S}_3\mathbf{L}_{\text{out}}} \hat{\mathbf{L}}_{\text{out}} \times \hat{\mathbf{S}}_3, \quad (\text{A3})$$

where the orbit-averaged precession rates are

$$\Omega_{\mathbf{L}_{\text{out}}\mathbf{S}_3} = \frac{GS_3(4 + 3m_{12}/m_3)}{2c^2 a_{\text{out}}^3 (1 - e_{\text{out}}^2)^{3/2}} = \Omega_{\mathbf{S}_3\mathbf{L}_{\text{out}}} \frac{S_3}{L_{\text{out}}}. \quad (\text{A4})$$

Since in our case, \mathbf{S}_3 can be easily larger than \mathbf{L}_{out} , the de-Sitter precession (Eq. [A3](#)) is negligible.

(ii) *Effect II: Precession of \mathbf{L}_{in} around \mathbf{L}_{out} .* In addition to the Newtonian precession (driven by the tidal potential of m_3), \mathbf{L}_{in} experiences an additional de-Sitter like (geodesic) precession in the gravitational field of m_3 introduced by

GR. This is a 1.5 PN spin-orbit coupling effect, with \mathbf{L}_{in} behaving like a “spin”. We have

$$\left. \frac{d\mathbf{L}_{\text{in}}}{dt} \right|_{\mathbf{L}_{\text{in}}\mathbf{L}_{\text{out}}} = \Omega_{\mathbf{L}_{\text{in}}\mathbf{L}_{\text{out}}}^{(\text{GR})} \hat{\mathbf{L}}_{\text{out}} \times \mathbf{L}_{\text{in}}, \quad (\text{A5})$$

$$\left. \frac{d\mathbf{e}_{\text{in}}}{dt} \right|_{\mathbf{L}_{\text{in}}\mathbf{L}_{\text{out}}} = \Omega_{\mathbf{L}_{\text{in}}\mathbf{L}_{\text{out}}}^{(\text{GR})} \hat{\mathbf{L}}_{\text{out}} \times \mathbf{e}_{\text{in}}, \quad (\text{A6})$$

and the feedback from $\hat{\mathbf{L}}_{\text{in}}$, \mathbf{e}_{in} on \mathbf{L}_{out} and \mathbf{e}_{out} are given by (e.g., [Barker & O’Connell 1975](#))

$$\left. \frac{d\mathbf{L}_{\text{out}}}{dt} \right|_{\mathbf{L}_{\text{out}}\mathbf{L}_{\text{in}}} = \Omega_{\mathbf{L}_{\text{out}}\mathbf{L}_{\text{in}}}^{(\text{GR})} \hat{\mathbf{L}}_{\text{in}} \times \mathbf{L}_{\text{out}}, \quad (\text{A7})$$

$$\begin{aligned} \left. \frac{d\mathbf{e}_{\text{out}}}{dt} \right|_{\mathbf{L}_{\text{out}}\mathbf{L}_{\text{in}}} &= \Omega_{\mathbf{L}_{\text{out}}\mathbf{L}_{\text{in}}}^{(\text{GR})} \hat{\mathbf{L}}_{\text{in}} \times \mathbf{e}_{\text{out}} \\ &\quad - 3\omega_{\mathbf{L}_{\text{out}}\mathbf{L}_{\text{in}}}^{(\text{GR})} (\hat{\mathbf{L}}_{\text{out}} \cdot \hat{\mathbf{L}}_{\text{in}}) \hat{\mathbf{L}}_{\text{out}} \times \mathbf{e}_{\text{out}}, \end{aligned} \quad (\text{A8})$$

with

$$\Omega_{\mathbf{L}_{\text{in}}\mathbf{L}_{\text{out}}}^{(\text{GR})} = \frac{3}{2} \frac{G(m_3 + \mu_{\text{out}}/3)n_{\text{out}}}{c^2 a_{\text{out}}(1 - e_{\text{out}}^2)} = \Omega_{\mathbf{L}_{\text{out}}\mathbf{L}_{\text{in}}}^{(\text{GR})} \frac{L_{\text{out}}}{L_{\text{in}}}, \quad (\text{A9})$$

where $n_{\text{out}} = (Gm_{\text{tot}}/a_{\text{out}}^3)^{1/2}$.

(iii) *Effect III: Precession of \mathbf{L}_{in} around \mathbf{S}_3 .* Since the semimajor axis of the inner orbit (a_{in}) is much smaller than the outer orbit (a_{out}), the inner binary can be treated as a single body approximately. Therefore, the angular momentum \mathbf{L}_{in} is coupled to the spin angular momentum \mathbf{S}_3 of m_3 , and experiences Lens-Thirring precession. This is a 2 PN spin-spin coupling effect, with \mathbf{L}_{in} behaving like a “spin”. We have

$$\begin{aligned} \left. \frac{d\mathbf{L}_{\text{in}}}{dt} \right|_{\mathbf{L}_{\text{in}}\mathbf{S}_3} &= \Omega_{\mathbf{L}_{\text{in}}\mathbf{S}_3} \hat{\mathbf{S}}_3 \times \mathbf{L}_{\text{in}} \\ &\quad - 3\Omega_{\mathbf{L}_{\text{in}}\mathbf{S}_3} (\hat{\mathbf{L}}_{\text{out}} \cdot \hat{\mathbf{S}}_3) \hat{\mathbf{L}}_{\text{out}} \times \mathbf{L}_{\text{in}}, \end{aligned} \quad (\text{A10})$$

$$\begin{aligned} \left. \frac{d\mathbf{e}_{\text{in}}}{dt} \right|_{\mathbf{L}_{\text{in}}\mathbf{S}_3} &= \Omega_{\mathbf{L}_{\text{in}}\mathbf{S}_3} \hat{\mathbf{S}}_3 \times \mathbf{e}_{\text{in}} \\ &\quad - 3\Omega_{\mathbf{L}_{\text{in}}\mathbf{S}_3} (\hat{\mathbf{L}}_{\text{out}} \cdot \hat{\mathbf{S}}_3) \hat{\mathbf{L}}_{\text{out}} \times \mathbf{e}_{\text{in}}. \end{aligned} \quad (\text{A11})$$

The back-reaction on the outer binary gives (see Eqs. 64, 65, 70 of [Barker & O’Connell \(1975\)](#))

$$\begin{aligned} \left. \frac{d\mathbf{L}_{\text{out}}}{dt} \right|_{\mathbf{S}_3\mathbf{L}_{\text{in}}} &= -3\Omega_{\mathbf{S}_3\mathbf{L}_{\text{in}}} \left[(\hat{\mathbf{L}}_{\text{out}} \cdot \hat{\mathbf{L}}_{\text{in}}) \hat{\mathbf{S}}_3 + (\hat{\mathbf{L}}_{\text{out}} \cdot \hat{\mathbf{S}}_3) \hat{\mathbf{L}}_{\text{in}} \right] \\ &\quad \times \mathbf{L}_{\text{out}}, \end{aligned} \quad (\text{A12})$$

$$\begin{aligned} \left. \frac{d\mathbf{e}_{\text{out}}}{dt} \right|_{\mathbf{S}_3\mathbf{L}_{\text{in}}} &= -3\Omega_{\mathbf{S}_3\mathbf{L}_{\text{in}}} \left\{ (\hat{\mathbf{L}}_{\text{out}} \cdot \hat{\mathbf{L}}_{\text{in}}) \hat{\mathbf{S}}_3 + (\hat{\mathbf{L}}_{\text{out}} \cdot \hat{\mathbf{S}}_3) \hat{\mathbf{L}}_{\text{in}} \right. \\ &\quad \left. + [(\hat{\mathbf{L}}_{\text{in}} \cdot \hat{\mathbf{S}}_3) - 5(\hat{\mathbf{L}}_{\text{out}} \cdot \hat{\mathbf{L}}_{\text{in}})(\hat{\mathbf{L}}_{\text{out}} \cdot \hat{\mathbf{S}}_3)] \hat{\mathbf{L}}_{\text{out}} \right\} \\ &\quad \times \mathbf{e}_{\text{out}}. \end{aligned} \quad (\text{A13})$$

In the above, the orbit-averaged precession rates are

$$\Omega_{\mathbf{L}_{\text{in}}\mathbf{S}_3} = \frac{GS_3}{2c^2 a_{\text{out}}^3 (1 - e_{\text{out}}^2)^{3/2}} = \Omega_{\mathbf{S}_3\mathbf{L}_{\text{in}}} \frac{L_{\text{out}}}{L_{\text{in}}}. \quad (\text{A14})$$

B: MODIFIED EVOLUTION OF $\hat{\mathbf{L}}_{\text{in}}$ DUE TO SMBH SPIN

We explore the effect of the SMBH spin on the variation of orbital axis $\hat{\mathbf{L}}_{\text{in}}$ and eccentricity e_{in} , taking into account the full range of misalignment angle α (and χ_3). The results are shown in Figs. 5, 6 and 7.

C: SIGNAL-TO-NOISE RATIO

An individual binary generates a GW strain composed of discrete harmonics

$$h(t) = \sum_{n=1}^{\infty} h_n(f_n) e^{i2\pi f_n t}, \quad (\text{C1})$$

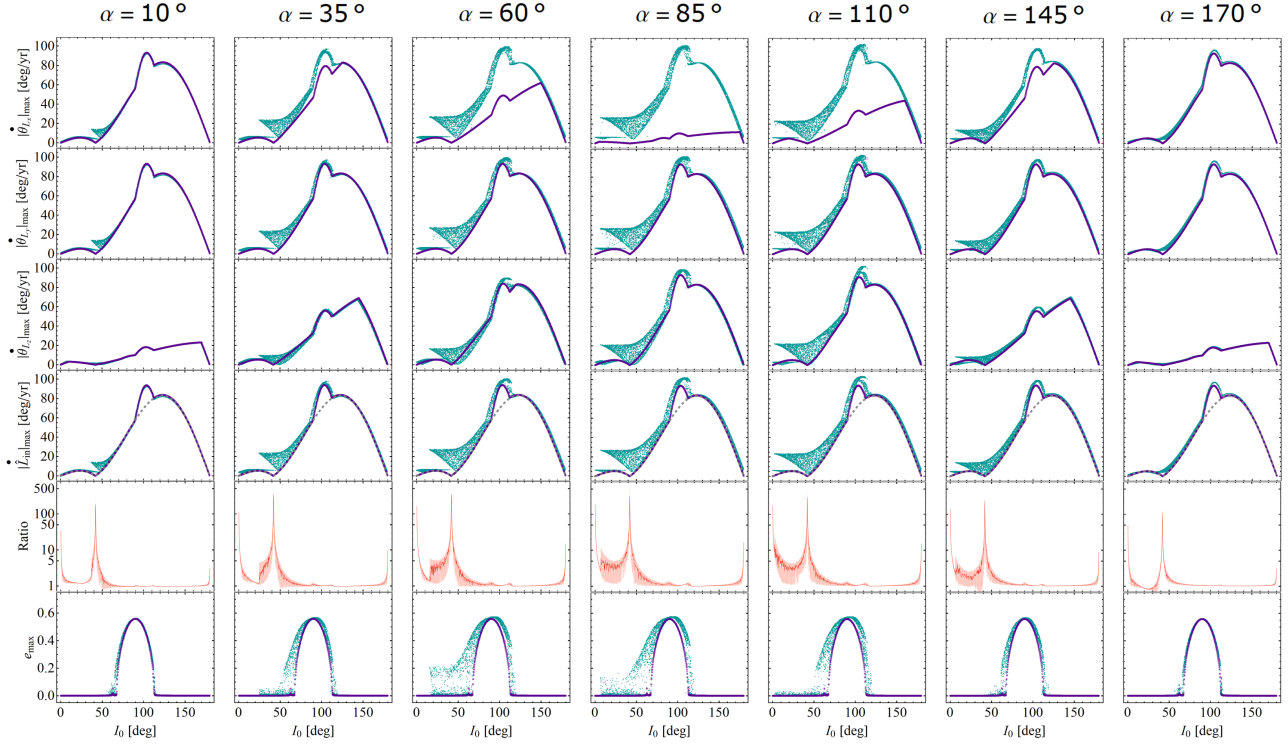


FIG. 5.— Similar to Fig. 4 in the main text, but we consider various values of α (as indicated). The fifth row shows the ratio $|\dot{\mathbf{L}}_{\text{in}}|_{\text{max}}(\chi_3 = 1)/|\dot{\mathbf{L}}_{\text{in}}|_{\text{max}}(\chi_3 = 0)$ as a function of I_0 , where the shaded region is obtained from the distribution of $|\dot{\mathbf{L}}_{\text{in}}|_{\text{max}}(\chi_3 = 1)$ shown in the fourth row, and the solid line corresponds to the mean value.

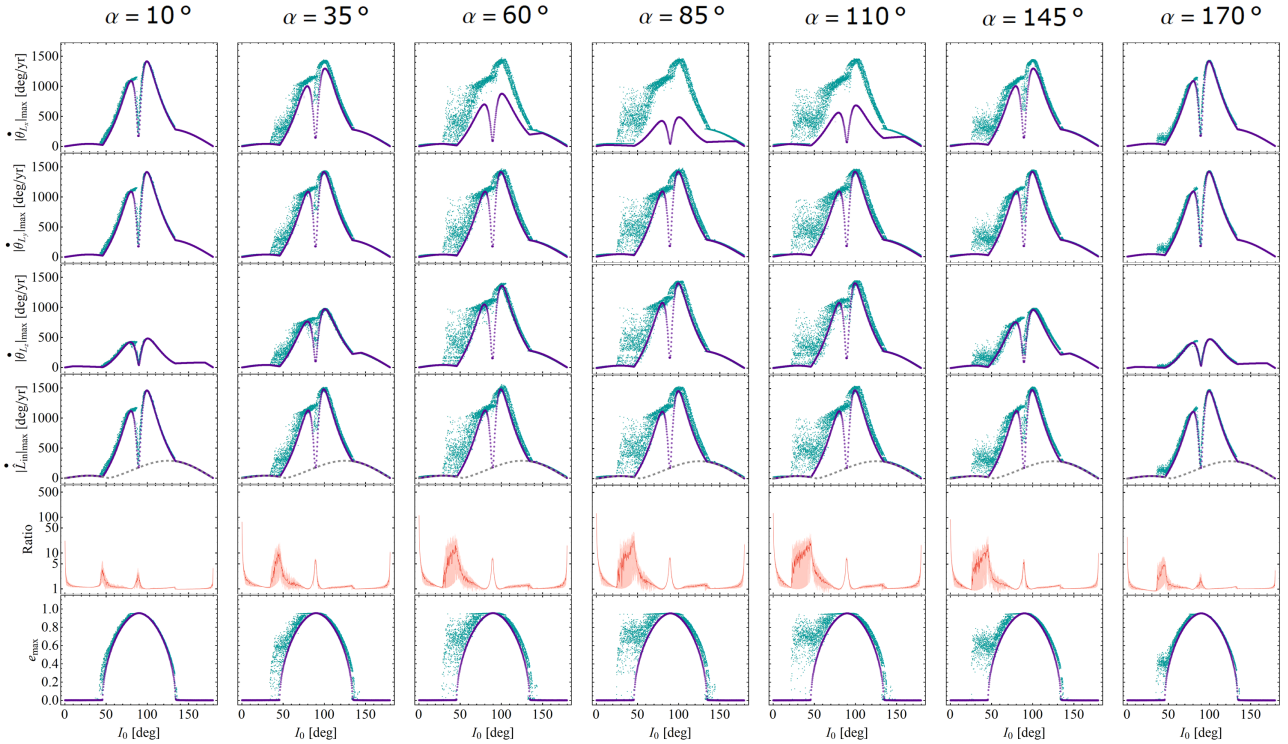


FIG. 6.— Similar to Fig. 5, but for the outer binary with $a_{\text{out}} = 10\text{AU}$.

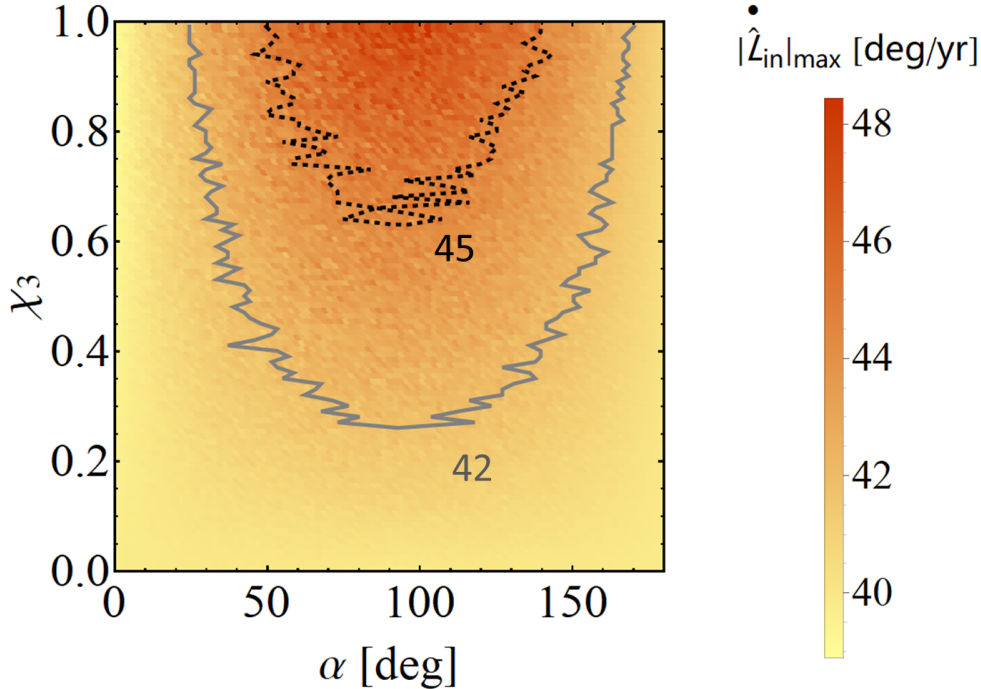


FIG. 7.— Values of the maximum rate of change of $|\dot{\mathbf{L}}_{\text{in}}|$ in $\chi_3 - \alpha$ plane. The system parameters are from the example in Fig. 2 (A) in the main text. For each combination of (χ_3, α) , we carry out 100 integrations with a uniform distribution of I_0 , and plot the median values of $|d\dot{\mathbf{L}}_{\text{in}}/dt|_{\text{max}}$. The two lines (gray dashed and black solid) specify $|d\dot{\mathbf{L}}_{\text{in}}/dt|_{\text{max}} = 42^\circ/\text{yr}, 45^\circ/\text{yr}$, respectively.

where n is the number of the harmonics. The frequency harmonic is $f_n = n f_{\text{orb}}$, $f_{\text{orb}} \equiv \sqrt{Gm_{12}/a^3}/2\pi$, and

$$h_n(f_n) = \frac{2}{n} \sqrt{g(n, e_{\text{in}})} h_0, \quad (\text{C2})$$

here, the function $g(n, e_{\text{in}})$ is given by

$$g(n, e_{\text{in}}) = \frac{n^4}{32} \left[\left(J_{n-2} - 2e_{\text{in}} J_{n-1} + \frac{2}{n} J_n + 2e_{\text{in}} J_{n+1} - J_{n+1} \right)^2 + (1 - e_{\text{in}}^2) (J_{n-2} - 2J_n + J_{n+2})^2 + \frac{4}{3n^2} J_n^2 \right] \quad (\text{C3})$$

with $J_n \equiv J_n(x)$ is the i th Bessel function evaluated at $x = ne_{\text{in}}$. Note that we have introduced the root-mean-square (rms) strain amplitude for the circular orbit at distance D

$$h_0 = \sqrt{\frac{32}{5}} \frac{G^2 m_1 m_2}{c^4 D a_{\text{in}}}. \quad (\text{C4})$$

The prefactor $\sqrt{32/5}$ accounts for rms averaging the GW strain over inclination. Since we only consider the BHB mergers in our MW, Equation (C4) has no redshift dependence.

The signal-to-noise ratio (SNR) is evaluated by

$$\langle S/N \rangle^2 \equiv \int_0^\infty \frac{4|\tilde{h}(f)|^2}{S_n(f)} df \quad (\text{C5})$$

here

$$\tilde{h}(f) = \sum_{n=1}^{\infty} h_n(f_n) T_{\text{obs}} \text{sinc}[\pi(f - f_n) T_{\text{obs}}], \quad (\text{C6})$$

T_{obs} is the observation time, and $S_n(f)$ is the full strain spectral sensitivity density. Here, we consider the LISA instrumental noise and confusion noise from the unresolved galactic binaries (e.g., Robson et al. 2019).

If the system has the orbital decay timescale much longer than the LISA mission time, we have

$$\langle S/N \rangle^2 = \sum_{n=1}^{\infty} \frac{4|h_n(f_n)|^2 (f_n T_{\text{obs}})}{f_n S_n(f_n)}. \quad (\text{C7})$$

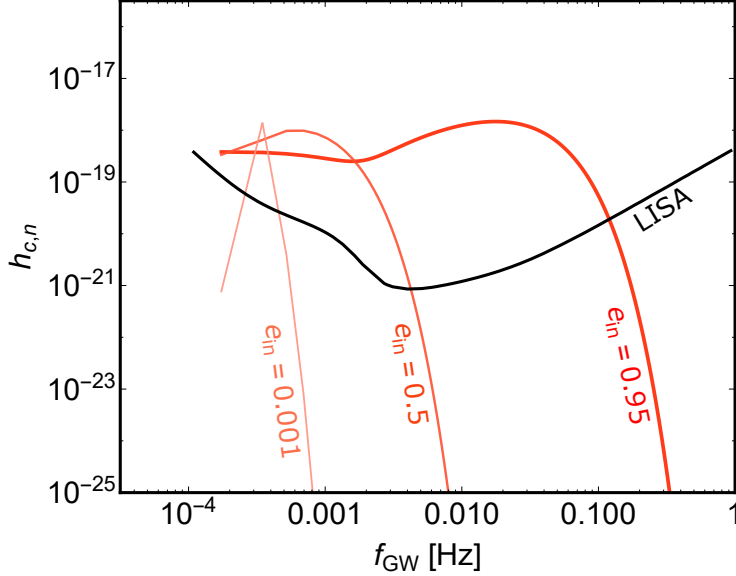


FIG. 8.— The GW strain curve of BH binary ($m_1 = 20M_\odot$, $m_2 = 10M_\odot$ and $a_{\text{in}} = 0.01\text{AU}$). Different orbital eccentricities are taken into account (as labeled). The red curves are obtained by Eq. (C8) with a series of n , and the spectral sensitivity density of LISA is from Robson et al. (2019).

Also, we can define the characteristic strain as

$$h_{c,n} = 2h_n(f_n)\sqrt{f_n T_{\text{obs}}}. \quad (\text{C8})$$

Equations (C7)-(C8) suggest that SNR can be enhanced by a factor of $\sqrt{f_n T_{\text{obs}}}$.

We find that for the GW sources ($m_1 = 20M_\odot$, $m_2 = 10M_\odot$ and $a_{\text{in}} = 0.01\text{AU}$), the total SNR is greater than 37 if we assume the observation time $T_{\text{obs}} = 5\text{yrs}$ and the distance $D = 8\text{kpc}$. An elliptic inner orbit can enhance the detectability, increasing the overall SNR by a factor of 10 (or even more), as shown in Fig. 8.

D: MODIFIED GW WAVEFORMS

As the compact binary precesses, both amplitude and phase of the GW waveform can be modified. The signature of the time-varying orientation $\hat{\mathbf{L}}_{\text{in}}$ can be extracted through projecting the GW radiation onto the antenna (detector) coordinates (e.g., Yu & Chen 2021).

Considering the circular inner orbit, the waveform is expressed in terms of frequency

$$\tilde{W}(f) = \Lambda(f)\tilde{W}_C(f), \quad (\text{D1})$$

where $\tilde{W}_C(f)$ is the antenna-independent “carrier”, which is a function of the chirp mass, distance, time and phase of coalescence, and

$$\Lambda(f) \equiv \sqrt{A_+^2(t)F_+^2(t) + A_\times^2(t)F_\times^2(t)} \times \exp\{-i[\Phi_p(t) + 2\Phi_T(t) + \Phi_D(t)]\}. \quad (\text{D2})$$

Here, we have introduced the amplitude terms

$$A_+(t) = 1 + (\hat{\mathbf{L}}_{\text{in}}(t) \cdot \hat{\mathbf{N}})^2, \quad (\text{D3})$$

$$A_\times(t) = -2\hat{\mathbf{L}}_{\text{in}}(t) \cdot \hat{\mathbf{N}}, \quad (\text{D4})$$

where $\hat{\mathbf{N}}$ is the direction of line-of-sight, and $F_{+(\times)}(t)$ is the antenna pattern coefficient. For the phase terms, Φ_p shows the polarization phase

$$\Phi_p(t) = \arctan\left[-\frac{A_\times(t)F_\times(t)}{A_+(t)F_+(t)}\right], \quad (\text{D5})$$

Φ_T characterizes the Thomas precession

$$\Phi_T(t) = -\int dt \left[\frac{\hat{\mathbf{L}}_{\text{in}}(t) \cdot \hat{\mathbf{N}}}{1 - (\hat{\mathbf{L}}_{\text{in}}(t) \cdot \hat{\mathbf{N}})^2} \right] (\hat{\mathbf{L}}_{\text{in}}(t) \times \hat{\mathbf{N}}) \cdot \frac{d\hat{\mathbf{L}}_{\text{in}}(t)}{dt}, \quad (\text{D6})$$

and Φ_D is the Doppler phase induced by the motions of outer orbit (and/or the detector orbiting around the Sun).

Therefore, the change of the $\hat{\mathbf{L}}_{\text{in}}$ orientation can be tracked for the GW source with sufficient SNR. [Yu & Chen \(2021\)](#) explored the detectability of the precessing $\hat{\mathbf{L}}_{\text{in}}$ around $\hat{\mathbf{L}}_{\text{out}}$. In their study, the Newtonian precession and the de-Sitter like precession (Effect II here) are taken into account, and the evolution of $\hat{\mathbf{L}}_{\text{in}}$ is regular. It is suggested that the orientation change is measurable if the precession timescale is less than the observation time. Similarly, since the spin-induced precession timescale we considered is comparable or less than 10 yrs, the frame-dragging effect in the orbital plane might also be detected through the modified GW waveform—the only thing is $\hat{\mathbf{L}}_{\text{in}}$ evolves in a non-regular way.